

Effect of Structural Parameters on the Jet Formation and Penetration Capability of Small Caliber Shaped Charges

Yongjie XU*, Xiaodong WANG**, Wenhui XIE***, Nana ZHENG****

*College of Mechatronic Engineering, North University of China, 030051 Taiyuan, P.R. China,

E-mail: yongqiang515@nuc.edu.cn (Corresponding author)

**College of Mechatronic Engineering, North University of China, 030051 Taiyuan, P.R. China,

E-mail: wangxiaodongedu@foxmail.com

***Chongqing Hongyu Precision Industrial, 402760 Chongqing, P.R. China, E-mail: 13036317656@139.com

****Changzhi Military Representative Office of Beijing Military Representative Bureau, 046000 Changzhi, P.R. China,

E-mail: 1357093356@qq.com

<https://doi.org/10.5755/j02.mech.32649>

1. Introduction

A small-caliber, high-explosive anti-tank cartridge is a lethal weapon. It is proposed to fill the gap between grenade and mortar fire [1]. Its caliber is generally between 20 and 40 mm, with a certain anti-armor capability. The previous study reported that the penetration depth of a 40 mm series anti-armor cartridge against rolled homogeneous armor was between 50 and 70 mm [2], which characteristic can be improved by adjusting structural parameters of small-caliber high-explosive anti-tank cartridges.

The penetration depth of the shaped charge jet is closely related to liner structure and material, effective jet length, target strength, detonation wave shape, and structural parameters. Copper liners have been manufactured using the electrodeposition technique with different average grain sizes. The breakup time and total number of shaped charge jets were determined for the range of copper liners of different grain sizes, and the determination of the velocity difference between jet fragments was studied [3]. The electrodeposition technique can produce electrolytic copper with the minimum amount of oxygen and sulfur elements used in the shaped charge liner. High-end stationary vacuum spectrometer was used to determine the elemental composition, and SEM was used to investigate the shape of copper texture inside the deposited layers and to determine the average grain size. The performance of the produced copper liner-shaped charge was investigated by the static test, where the penetration depth of the optimized electrolytic liner was enhanced by 22.7% compared to that of the non-optimized liner [4]. In calculating the shaped charge jet penetration, the effective jet length between a virtual origin point and the target surface is a crucial adjective. The firing test has validated the numerical approach for estimating the virtual origin point; the results show that the maximum difference in penetration depth between the experiment and that calculated by the approach is less than 4% [5]. The yield strength of the target can largely reduce the penetration depth of shaped charge jets. The shaped charge jet penetration depth prediction model is modified by introducing a target resistance reduction term. The numerical and experimental results show that the increased target's yield strength leads to a large decrease in jet penetration depth into targets [6]. The waveform shaper can affect the propagation path of the detonation wave and collide at the charge axis to form an overdriven detonation. Effective application in shaped

charges can obtain long rod damage elements with a large length-to-diameter ratio, greatly improving penetration performance [7]. The structural parameters of small-caliber ammunition liners (especially, their thickness and curvature radius) significantly influence the jet forming characteristics, shape and velocity of damaged elements [8]. Based on the micro-shaped charge warhead, the penetration efficiencies of different micro-jets on gelatin targets were compared and analyzed. The numerical result shows that the micro-shaped charge nylon and teflon jets could pass through the gelatin target and transfer more energy to it than copper [9].

To analyze the damage efficiency of small-caliber high explosive anti-tank cartridges, we performed the numerical simulation and experimental study on the optimization design of shaped charge. The influence of warhead structural parameters on shaped charge jet forming and penetration capability was investigated, and the proposed scheme of small-caliber shaped charge structure was put forward. The research results provide theoretical and technical support for the design and engineering application of small-caliber high-explosive ammunition.

2. Analysis and modeling

2.1. Physical model

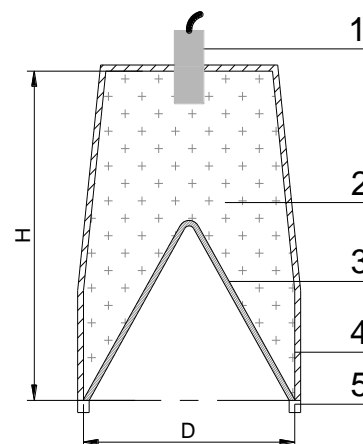


Fig. 1 Schematic diagram of a shaped charge: H is charge height, D is charge diameter, 1 is initiating explosive device, 2 is an explosive charge, 3 is a liner, 4 is warhead shell, and 5 is a dead ring

According to the ammunition design theory, a small-caliber high-explosive anti-tank cartridge warhead model was established using a 35 mm caliber projectile research platform. Its structural diagram is shown in Fig. 1.

2.2. Material models

Equation of state (EOS) of a material is an expression of density, pressure and temperature [10-12] and it is usually expressed as:

$$P = P(\rho, E), \quad (1)$$

where, P is pressure, ρ is density, and E is internal energy.

The relationship of internal energy and temperature is expressed as:

$$dE = c_v \cdot dT, \quad (2)$$

where, c_p is constant-volume specific heat, and T is temperature.

Air is ideal gas, and its EOS is expressed as following:

$$P_A = (\gamma - 1) \cdot \rho_A \cdot E_A, \quad (3)$$

where subscript A is for material air, $\rho_A = 1.225 \times 10^{-3} \text{ g/cm}^3$, $E_A = 0.2068 \times 10^3 \text{ kJ/m}^3$, c_p is constant-pressure specific heat, and $\gamma = c_p/c_v$ is specific heat ratio which value is 1.404.

The EOS of the explosive HMX is Jones-Wilkins-Lee (JWL) equation, and it is expressed as following:

$$P_{ex} = A \cdot \left(1 - \frac{\omega}{R_1 \cdot V_r}\right) \cdot e^{-R_1 \cdot V_r} + B \cdot \left(1 - \frac{\omega}{R_2 \cdot V_r}\right) \cdot e^{-R_2 \cdot V_r} + \frac{\omega \cdot E_{ex}}{V_r}, \quad (4)$$

where subscript ex is for explosive, V_r stands for the relative volume following the convention used in hydrodynamic codes, under the condition of specific volume, the value of V_r is equal to ρ/ρ_0 , and ρ_0 is loading density, ρ is density of detonation products.

In this equation, five parameters must be determined. A , B are the linear coefficients and R_1 , R_2 , ω are the non-linear coefficients. The values of the parameters are given in Table 1.

Table 1
The parameters of JWL EOS of explosive HMX

ρ , $\text{g}\cdot\text{cm}^{-3}$	E_{ex} , $\text{kJ}\cdot\text{m}^{-3}$	A , GPa	B , GPa	R_1	R_2	ω
1.891	1.05×10^7	778.280	7.071	4.200	1.000	0.300

The EOS of copper is shock model. These equations relate the pressure (P), internal energy (E), specific volume (V), or density (ρ) behind the shock wave to these same quantities in front of the shock wave in terms of the shock velocity (u_s) and the particle velocity (u_p) due to the

shock wave. These equations express the conservation of mass, momentum, and energy, and for a coordinate system in which the material in front of the shock wave is at rest. These equations are given as follows:

$$\rho_0 \cdot u_s = \rho \cdot (u_s - u_p), \quad (5)$$

$$P - P_0 = \rho_0 \cdot u_s \cdot u_p, \quad (6)$$

$$\left[(E - E_0) - \frac{u_p^2}{2} \right] \cdot \rho_0 \cdot u_s = P_0 \cdot u_p, \quad (7)$$

$$u_s = c_0 + s \cdot u_p, \quad (8)$$

where the subscript 0 refers to the initial state and is referred to as the centering point of the Hugoniot, c_0 is acoustic speed of sound volume, and s is a constant.

By using the linear $u_s - u_p$ Hugoniot, η is defined by:

$$\eta = (V_0 - V)/V_0 = 1 - \rho_0 \cdot V. \quad (9)$$

Combining this with mass conservation, yields:

$$\eta = u_p / u_s. \quad (10)$$

Conservation of momentum, yields to:

$$P_H = \rho_0 \cdot c_0^2 \cdot \eta / (1 - s \cdot \eta)^2. \quad (11)$$

The energy equation with E_0 equal to zero, yields to:

$$E_H = \eta \cdot P_H / 2 \cdot \rho_0. \quad (12)$$

For such calculations it is convenient to work through the general energy-pressure equation as following:

$$E = E_H + (P - P_H) / (\rho \cdot \gamma). \quad (13)$$

The equation states that the pressure and energy at any particular volume can be related to these quantities on the Hugoniot, designated by the subscript H . γ is the Gruneisen parameter, and it is always considered to be in dependent of pressure and is usually determined from the relationship following:

$$\rho \cdot \gamma = \rho_0 \cdot \gamma_0, \quad (14)$$

where subscript 0 represents room-temperature and zero-pressure value.

The parameters of shock EOS of copper are given in Table 2.

Table 2
The parameters of Shock EOS of copper

Material	EOS	ρ , $\text{g}\cdot\text{cm}^{-3}$	γ	c_0 , $\text{cm}\cdot\mu\text{s}^{-1}$	s
Copper	Shock	8.930	1.990	0.394	1.489

Material is of a warhead shell and target is steel 4340. The strength model is also depicted by Johnson-Cook (J-C) equation model, which is widely used in practical applications. It allows to assess the effective stress $\bar{\sigma}$ as following:

$$\bar{\sigma} = \left[A_1 + B_1 \cdot (\bar{\varepsilon}_p)^n \right] \cdot \left(1 + C_1 \cdot \ln \dot{\varepsilon}^* \right) \cdot \left[1 - \left(\frac{T - T_r}{T - T_m} \right)^m \right], \quad (15)$$

where $\bar{\varepsilon}_p$ is equivalent plastic strain, $\dot{\varepsilon}^*$ is dimensionless plastic strain rate, T is process temperature, T_r is ambient temperature, T_m is melting temperature, and the parameters A_1 , B_1 , C_1 , n , m are the five material constants. And, A_1 is yield stress, B_1 is hardening constant, C_1 is strain rate constant, n is hardening exponent, m thermal softening exponent. The parameters of J-C model of steel 4340 are given in Table 3.

Table 3

The parameters of J-C model of steel 4340

A_1 , MPa	B_1 , MPa	C_1	n	m	T_r , K	T_m , K
792	510	0.014	0.260	1.030	300	1793

2.3. Finite element model

The finite element model of small-caliber armor-piercing warhead was established and realized via the ANSYS AUTODYN explosive mechanics analysis software [13], and the process of shaped charge jet forming and penetrating target was simulated in the cm-g- μ s unit system.

In the simulation of shaped charge jet forming and penetration, the Euler algorithm was used to describe the large deformation process of materials, including HMX, liner, and air. The Lagrangian algorithm was used to describe the deformation of the steel target accurately. The fluid structure coupling algorithm was used to simulate the mutual coupling of the Euler and Lagrange units.

Due to the symmetry of the shaped charge

structure, an axisymmetric model was adopted for numerical simulation. The size of the Euler domain was 60 mm×300 mm, the size of the steel target was 100 mm×150 mm, and both mesh sizes were 0.5 mm×0.5 mm. The FLOW_OUT subroutine was added to the air domain's boundary region to reduce the shock wave's reflection and simulate the infinite air domain in real situations.

To improve the numerical simulation accuracy, finite element models with different grid quantities and mesh sizes were used. The numerical simulation results gradually converged when the mesh size was gradually reduced to 0.5 mm. Still, the smaller mesh size greatly increased the number of grids and computation scope, reducing the computing efficiency. Therefore, the calculation efficiency and accuracy were balanced at a mesh size of 0.5 mm. The calculation results of grid quality verification are shown in Fig. 2.

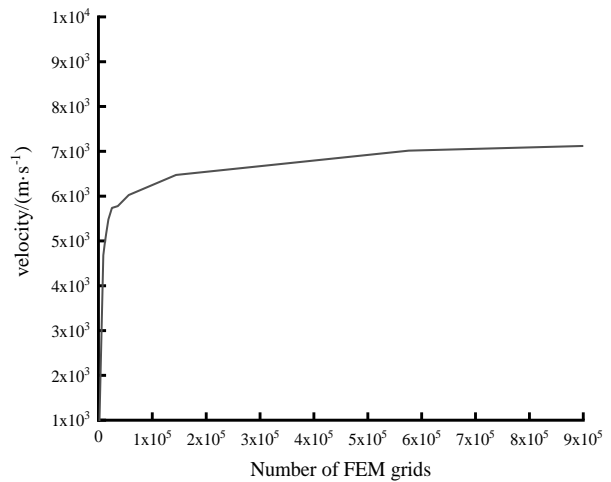


Fig. 2 Change rule about jet velocity and grid quality

In Fig. 3, the air domain, explosive charge, and liner are shown in blue, green, and red colors, respectively; the initiation point is depicted by a diamond symbol, and the numbers 1 to 6 are Gaussian points. The initiation mode is the center point initiation.

The steel 4340 target model was established to study the penetration capability, as shown in Fig. 4.

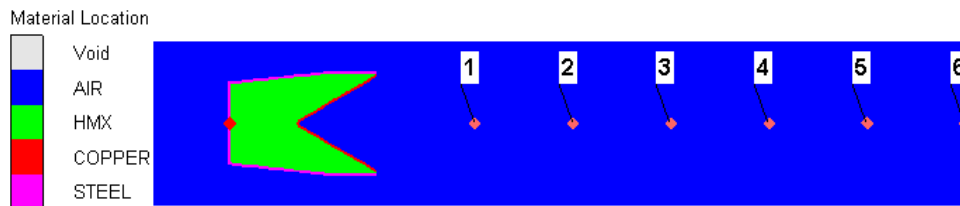


Fig 3 Finite element model of shaped charge

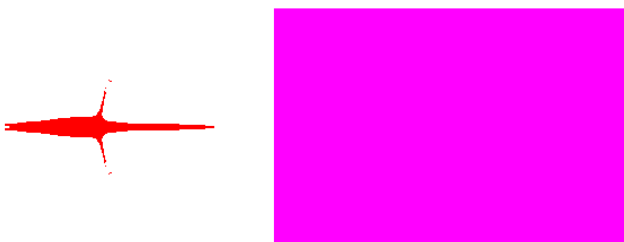


Fig. 4 Model of shaped charge jet penetrating the target

3. Figures and tables

Orthogonal optimization design quantitatively analyzes the relationship between parameter combination and system characteristics by statistical methods to determine the system's optimal parameter combination [14-15].

The three-factor and three-level optimization design was selected. The levels of each factor are shown in Table 4.

The orthogonal optimization design scheme and calculation results are summarized in Table 5.

The key indicator of the percentage of effective mass (PEM) is the ratio of the shaped charge jet's effective mass to the liner's total mass. In this work, the effective mass is the mass of the part of jet velocity above 2000 m/s.

It can be seen from the simulation results that the decreasing order for factor 1 is $\bar{K}_{11} > \bar{K}_{21} > \bar{K}_{31}$; for factor 2, it is $\bar{K}_{32} > \bar{K}_{22} > \bar{K}_{12}$, and for factor 3, it is $\bar{K}_{33} > \bar{K}_{23} > \bar{K}_{13}$.

The key indicator of the percentage of effective mass (PEM) is the ratio of the shaped charge jet's effective mass to the liner's total mass. In this work, the effective mass is the mass of the part of jet velocity above 2000 m/s.

Table 4
Factors and levels of orthogonal experiment

Level	Factors		
	liner thickness δ , mm	liner cone angle 2α , °	H/D
1	0.9	40	1.1
2	1.0	50	1.3
3	1.1	60	1.5

Table 5
Experimental scheme and results

SN	A	B	C	PEM
	δ , mm	2α , °	H/D	
1	0.9	40	1.1	0.2079
2	0.9	50	1.3	0.2948
3	0.9	60	1.5	0.3957
4	1	40	1.3	0.1981
5	1	50	1.5	0.2844
6	1	60	1.1	0.3439
7	1.1	40	1.5	0.1976
8	1.1	50	1.1	0.2580
9	1.1	60	1.3	0.3418
K_1	0.8984	0.6036	0.8098	
K_2	0.8264	0.8372	0.8347	
K_3	0.7974	1.0813	0.8777	
\bar{K}_1	0.2995	0.2012	0.2699	
\bar{K}_2	0.2755	0.2791	0.2782	
\bar{K}_3	0.2658	0.3604	0.2926	
R	0.0336	0.1592	0.0226	

It can be seen from the simulation results that the decreasing order for factor 1 is $\bar{K}_{11} > \bar{K}_{21} > \bar{K}_{31}$; for factor 2, it is $\bar{K}_{32} > \bar{K}_{22} > \bar{K}_{12}$, and for factor 3, it is $\bar{K}_{33} > \bar{K}_{23} > \bar{K}_{13}$.

Therefore, the optimal combination scheme of structural parameters of small-caliber high-explosive anti-tank cartridge was derived as $A_1B_3C_3$.

The range calculation result is $R_2 > R_1 > R_3$, indicating that among all parameters, the liner cone angle has the greatest effect on the jet formation, the liner thickness is the second, and the charge aspect ratio is the last.

The numerical simulation of the jet forming process was performed to verify the orthogonal optimization design result under the liner angle of 60° , liner thickness of 0.9 mm, and charge aspect ratio of 1.5.

The velocity and continuity of the shaped charge

jet are closely related to the penetration capability. Therefore, the effective mass is put forward to evaluate the forming performance of the jet. The larger the effective mass of the jet, the higher the penetration ability.

The head velocity and length of the shaped charge jet will directly affect its penetration performance, and excessive head velocity will cause a large velocity gradient, which will exceed the plastic limit of the liner material in the jet forming process, resulting in fracture and then reducing the continuity and penetration ability of the shaped charge jet.

Fig. 5 shows the jet's profile at different moments formed by the optimized small-caliber shaped charge.

At the same travel distance of 1CD (where CD is charge diameter), the velocity of the jet was kept above 5700 m/s, and the velocity gradients were 119, 89, 65, 51, and 32 m/s. The specific characteristic quantities of these shaped charge jets are listed in Table 6.

Table 6
Characteristic quantity of shaped charge jet

Gauges	Maximum velocity, m/s	Velocity gradient difference, m/s
#1	6116	—
#2	5997	119
#3	5908	89
#4	5843	65
#5	5792	51
#6	5760	32

As seen from Table 6, when the total length of the jet reached 6CD, there was no obvious fracture point, indicating that the overall continuity of the jet was good. It shows that the jet formed by the optimized shaped charge structure has strong penetrating ability.

The shaped charge jet length diagram for different positions of gauges is plotted in Fig. 6. In the numerical simulation of the forming process, when the jet travel position reached 1, 2, 3, 4, 5, and 6 CD, the lengths of the continuous jet were 62, 95, 128, 166, 198, and 230 mm, respectively. At the same travel distance of 1CD, the growth gradient of the jet length varied from 33 to 38 mm, then reached 32 mm. The specific values are listed in Table 7.

When the jet length reached 5CD, the jet head velocity still exceeded 5700 m/s, but there was a more obvious potential necking-fracture trend. Considering the continuous extension of the interaction position between the jet element and the target in the penetrating process, the optimal blasting height ensuring stable penetration performance of the shaped charge jet was between 2CD and 4CD.

Numerical simulations of the shaped charge jet penetrating steel targets with different blasting heights were carried out to verify the proper selection of the optimal blasting height. Results show that the penetration depth increased with the blasting height and reached its maximum

Table 7
Characteristic length of shaped charge jet

Gauges	Length of jet, cm	Growth gradient of jet length, mm
#1	6.2	—
#2	9.5	33
#3	12.8	33
#4	16.6	38
#5	19.8	32
#6	23.0	32

blasting height. Results show that the penetration depth increased with the blasting height and reached its maximum when the optimal blast height was achieved. In the

numerical simulation, the shaped charge was in the best state and fully contributed to its effectiveness when the blasting height ranged from 3CD to 4CD.

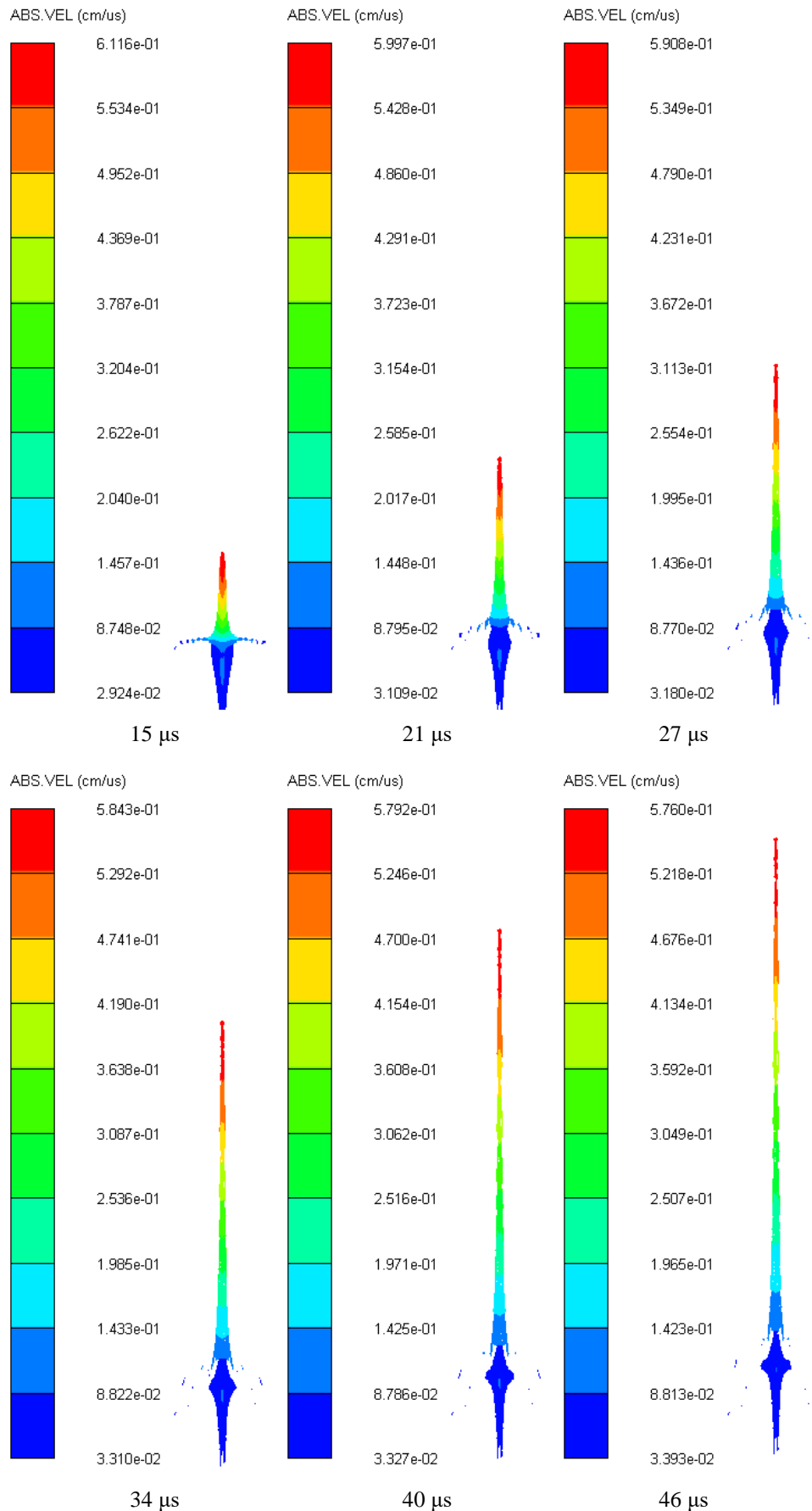


Fig. 5 Velocity nephogram of jet at different time moment

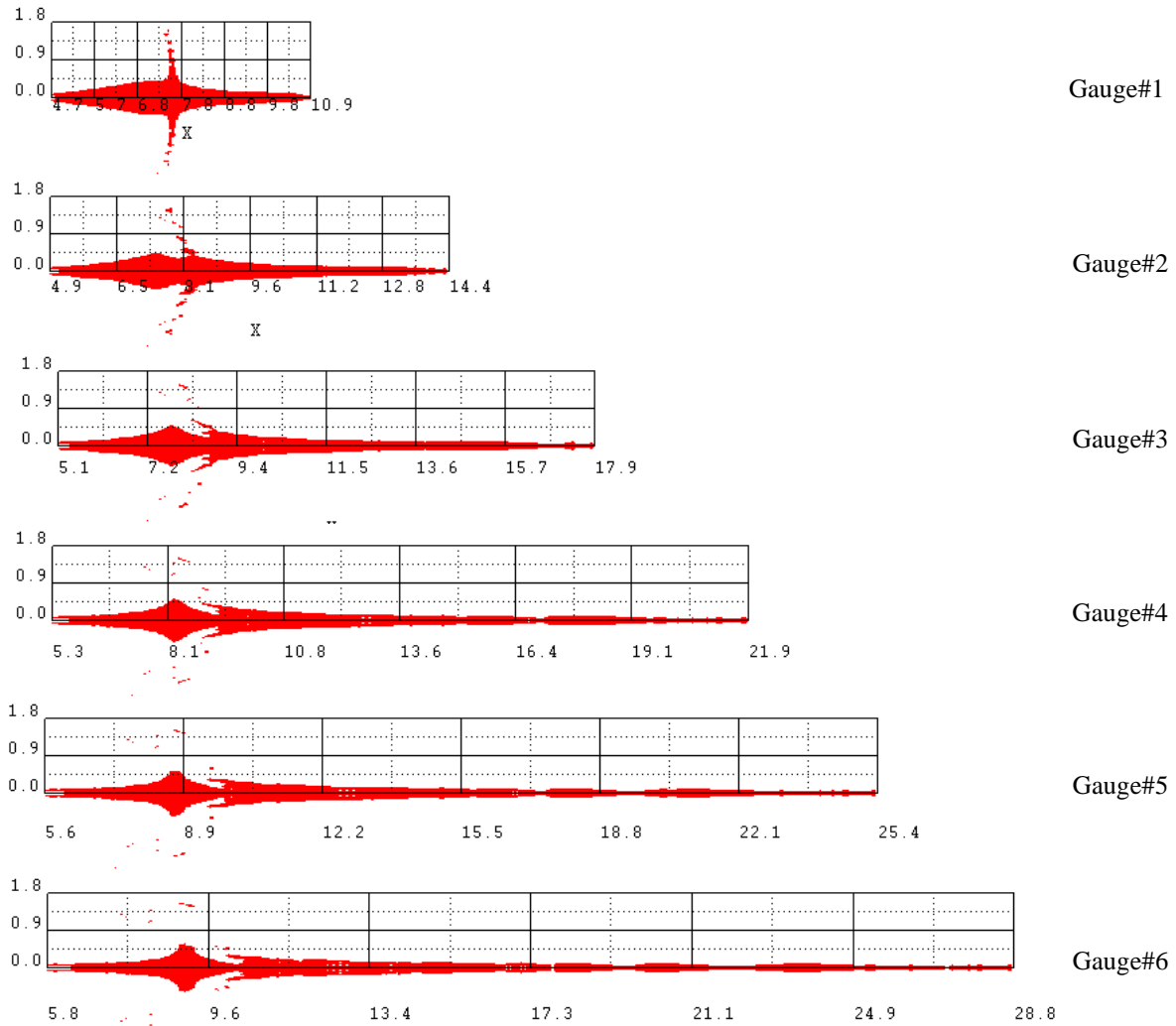


Fig. 6 Shaped charge jet morphology diagram, (units, cm)

To be consistent with the previous study, we determined that if the maximum speed of the shaped charge jet dropped below 2000 m/s, it lost its penetration ability. The variation trends of penetration depth and blasting heights are shown in Fig. 7.

The numerical simulation of jet penetration on the target at a 3CD blasting height was carried out to explore

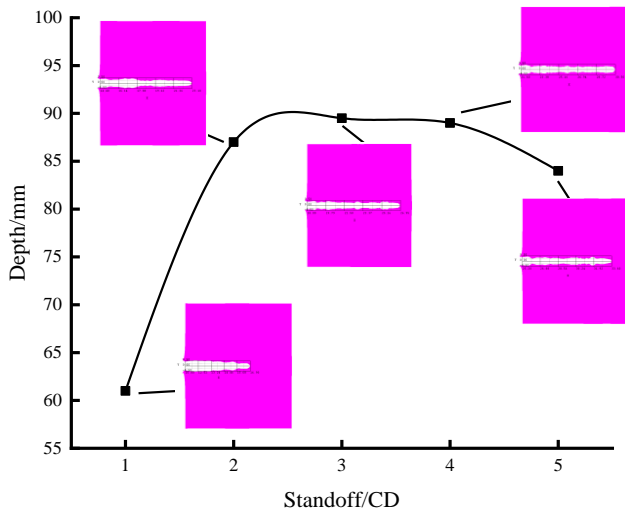


Fig. 7 Change trend of penetration depth and blasting heights

the maximum penetration capacity of the shaped charge jet structure. The penetration process of the shaped charge jet into a target is shown in Fig. 8.

At 10 μ s, the shaped charge jet was about to touch the target plate, and at 20-40 μ s, a stable jet penetration into the steel target was observed. During this period, the jet penetration rate was the highest. At 50 μ s, the pestle body separated from the main shaped charge jet. At the time of 60 μ s, it entered the end of penetration capacity until the jet kinetic energy was consumed and the penetration process ended.

The numerical simulation results showed that the penetration depth of a small-caliber shaped charge increased first and then decreased with standoff. When the explosion height exceeded the optimal standoff, the shaped charge jet continuously elongated with the increased jet's forward travel distance. When the length of the shaped charge jet exceeded the plastic limit of the liner material, the jet broke, and its penetration depth was greatly reduced. When the actual explosion height was less than the optimal standoff, the shaped charge jet touched the target before fully stretching, and the penetration kinetic energy failed to be fully utilized, resulting in the reduction of penetration depth. Thus, the maximum penetration depth corresponded to the optimum standoff.

Figure 9 shows a half of the axisymmetrical model of the shaped charge jet penetrating the target with a maximum depth of 105 mm.

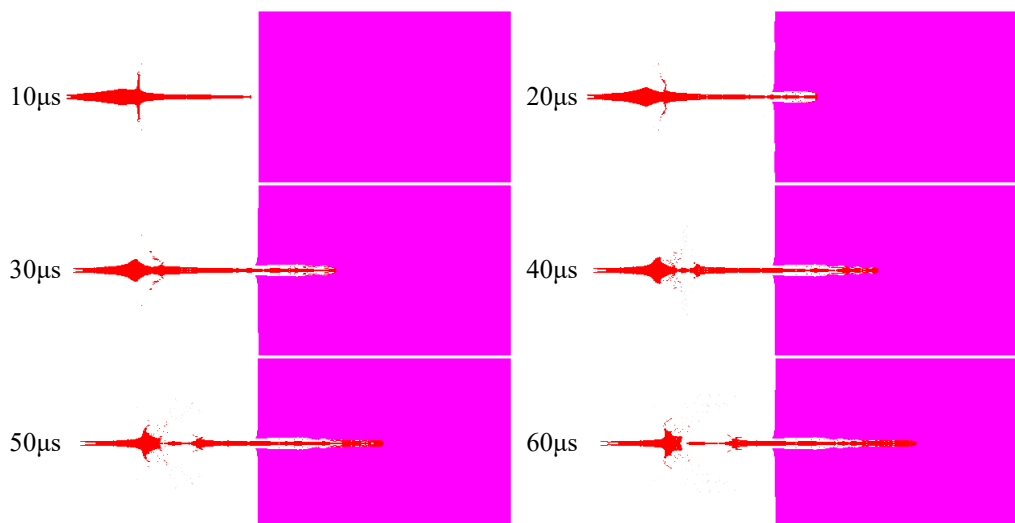


Fig. 8 Process of shaped charge jet penetration into steel target

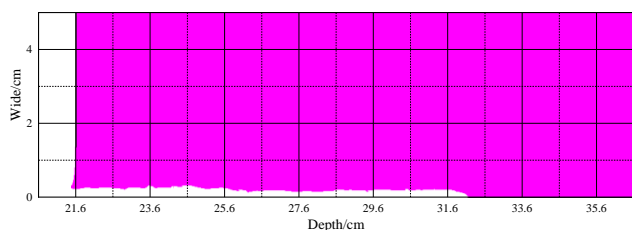


Fig. 9 A 1/2 model of the target penetration with a maximum depth of 105 mm

4. Explosion test

The explosion test was carried out according to the optimized warhead structure. The schematic diagram of the explosion test implementation plan is shown in Fig. 10.

According to the similar mechanical properties of steel 4340 and 45# [16-17], the material of targets used in experiments was 45# steel. In the experimental test, the target size was $\varnothing 120 \text{ mm} \times 100 \text{ mm}$ and the base plate size was $\varnothing 120 \text{ mm} \times 50 \text{ mm}$. The explosion test layout is given in Fig. 11.

To accurately display the internal penetration path, the post-experimental steel targets were cut by machining into halves. The results are shown in Fig. 12.

Experimental results of penetration depth are listed in Table 8.

The explosion test revealed that the maximum penetration depth of the shaped charge jet into a 45# steel target was 100 mm, and its average value was 86.67 mm. The minimum and average relative errors between numerical simulation and test results were 4.76% and 17.46%, respectively.

Table 8

Characteristic quantity of shaped charge jet

SN	Target serial number	Stand off	Penetration depth, mm
1	1-1#	3D	100
2	4-1#		100
3	9-1#		60
Average value			86.67

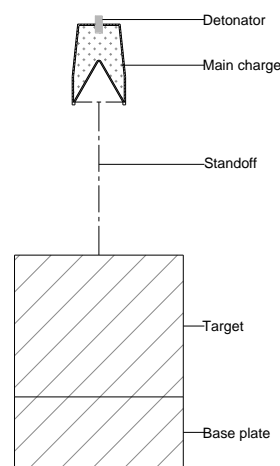


Fig. 10 Schematic diagram for test

5. Conclusions

The penetration capability of a shaped charge jet is a systematic problem closely related to the structural parameters of the charge liner, explosive charge parameters, and blasting height. Based on the application of a small-caliber shaped charge, the design scheme of a shaped charge warhead was proposed in this study, and numerical simulation and experimental research on the problems related to penetration capability were carried out.

In the present paper, the effects of structural parameters (including liner angle, liner thickness, and charge aspect ratio) on the shaped charge jet forming and penetration capability into steel targets were numerically simulated and experimentally verified. The following conclusions were drawn:

1. The shape charge jet's formability is controlled by the coupled effects of liner angle, liner thickness, and charge aspect ratio. The results of the orthogonal optimization design showed that the liner cone angle had the greatest effect, the liner thickness was secondary, and the charge aspect ratio was the least influencing factor.

2. During the explosion test, the charge liner collapsed, deformed, converged in the axis direction, and gradually formed the penetration body with continuous

morphology and velocity gradient. In motion deformation, the jet stretched and extended to achieve the best matching between shaping attitude, velocity, and length. At some instant, the stable forming shape of the jet corresponded to an optimal blasting height, and its penetration capability was the best. Due to the elastoplastic properties of the liner material, the optimum blasting height ranged. The smaller value should be determined as the best blasting height for further research because the increase in blasting height will dissipate the jet's kinetic energy. In this paper, the optimal blasting height range for the proposed small-caliber shaped charge structure ranged from three to four charge diameters,

which was verified by the explosion test.

3. In the explosion test, the average penetration depth of the proposed scheme of small-caliber shaped charge into steel targets was 86.67mm, and the relative average error between numerical simulation and experiment was 17.46%. It proved the validity of the proposed algorithm, parameter setting accuracy, and results' reliability.

4. Future research could consider other types of explosive charge, liner materials, processing technologies, and grain sizes of materials. More comprehensive theoretical research can provide solid theoretical support for the engineering application of shaped charge technology.



a

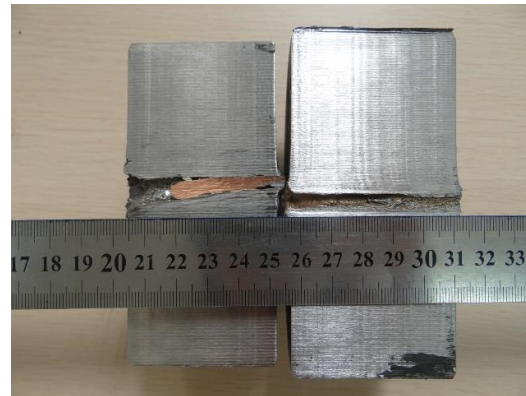


b



c

Fig. 11 Layout of static explosive experiment: a – SN1, b – SN2, c – SN3



a



b



c

Fig. 12 Penetration trajectory of post-experiment targets: a – 1-1#, b – 4-1#, c – 9-1#

Conflict of interests

The authors declare that there is no conflict of interests regarding the publication of this paper.

Acknowledgments

The authors would like to acknowledge the financial support from the project supported by the Foundation Research Project of Shanxi Province under Grant No.2021690 and Scientific and Technological Innovation Project of Shanxi Province under Grant No.2020299.

References

1. **Yin, J. P.; Wang, Z. J.** 2014. *Ammunition Theory*, Beijing Institute of Technology Press. 590 p. (in Chinese).
2. **Yin, J. P.** 2012. *Multiple Explosively Formed Projectile Warhead Technology*, National Defence Industry Press. 191p. (in Chinese).
3. **Elshenawy, T.** 2016. Determination of the Velocity Difference between Jet Fragments for a Range of Copper Liners with Different Small Grain Sizes, *Propellants Explosives Pyrotechnics* 41(1): 69-75. <https://doi.org/10.1002/prop.201500095>.
4. **Elshenawy, T.; Soliman, S.; Hawwas, A.** 2017. Influence of Electric Current Intensity on the Performance of Electroformed Copper Liner for Shaped Charge Application, *Defence Technology* 13(6): 439-442. <https://doi.org/10.1016/j.dt.2017.05.015>.
5. **Elshenawy, T.; Elbeih, A.; Klapotke, T. M.** 2018. A Numerical Method for the Determination of the Virtual Origin Point of Shaped Charge Jets Instead of Using Flash X-ray Radiography, *Journal of Energetic Materials* 36(2): 127-140. <https://doi.org/10.1080/07370652.2017.1324532>.
6. **Elshenawy, T.; Elbeih, A.; Li, Q. M.** 2018. Influence of Target Strength on the Penetration Depth of Shaped Charge Jets into RHA Targets, *International Journal of Mechanical Sciences* 136: 234-242. <https://doi.org/10.1016/j.ijmecsci.2017.12.041>.
7. **Liu, Y.K.; Yin, J.P.; Wang, Z.J.; Zhang, X.P.; Bi, G.J.** 2020. The EFP Formation and Penetration Capability of Double-Layer Shaped Charge with Wave Shaper, *Materials* 13(20): 4519. <https://doi.org/10.3390/ma13204519>.
8. **Ma, G.S.; He, G.L.; Liu, Y.K.; Guo, Y.C.** 2020. Study of the Forming Characteristics of Small-Caliber Ammunition with Circumferential MEFP, *Materials* 13(4): 891. <https://doi.org/10.3390/ma13040891>.
9. **Han, Y.Y.; Yin, J.P.; Wang, Z.J.; Li, X.D.; Bi, G.J.; Jia, Z.J.** 2022. Formability Characteristics and Penetration Performance of Micro-Jets from Different Materials, *Advances in Materials Science and Engineering* 2022: 2085108. <https://doi.org/10.1155/2022/2085108>.
10. **McQueen, R.G.; Marsh, S.P.; Taylor, J.W.; Fritz, J.N.; Carter, W.J.** 1970. CHAPTER VII – The Equation of State of Solids from Shock Wave Studies, in *High-velocity Impact Phenomena*, ed. R. Kinslow. New York: Academic Press: 293-417. <https://doi.org/10.1016/B978-0-12-408950-1.50012-4>.
11. **Lee, E.; Horning, H.; Kury, J.** 1968. *Adiabatic Expansion of High Explosive Detonation Products*. Lawrence National Laboratory Report UCRI-50422.
12. **Johnson, G. R.; Cook, W. H.** 1983. A Constitutive Model and Data for Metals Subjected to Large Strains, High Strain Rates and High Temperature. *Proceedings of 7th Int. Symposium on Ballistics*, Netherland.
13. **ANSYS Inc.** 2016. *Autodyn Material Library: ANSYS R17.2*, USA.
14. **Wang, Y.S.; Li, W.B.; Huang, X.N.; Wang, X.M.** 2020. Orthogonal Design of the Liner Structure in Dual-Mode Charge Warhead, *Chinese Journal of High Pressure Physics* 34(4): 157-165. (in Chinese) <https://doi.org/10.11858/gywlyxb.20200537>.
15. **Liu, H.J.; Wang, W.L.; Miao, R.; Wu S.** 2018. Optimum Design of Annular Double Done Shaped Charge Structure, *Chinese Journal of High Pressure Physics* 32(6): 107-115. (in Chinese) <https://doi.org/10.11858/gywlyxb.20180539>.
16. **Xu, W. L.; Wang, C.; Chen, D. P.** 2019. The Jet Formation and Penetration Capability of Hypervelocity Shaped Charges, *International Journal of Impact Engineering* 132: 103337. <https://doi.org/10.1016/j.ijimpeng.2019.103337>.
17. **Wang, Y.F.; Wang, Z.J.; Xu, Y.J.; Jin, Z.** 2022. The Effect of Cylindrical Liner Material on the Jet Formation and Penetration Capability of Cylinder-Cone-Shaped Charge, *Materials* 15(10): 3511. <https://doi.org/10.3390/ma15103511>.

Y. Xu, X. Wang, W. Xie, N. Zheng

EFFECT OF STRUCTURAL PARAMETERS ON THE JET FORMATION AND PENETRATION CAPABILITY OF SMALL CALIBER SHAPED CHARGES

Summary

This study used a small caliber high explosive anti-tank cartridge as a research platform and established a model of a 35 mm diameter warhead with a copper liner. To this end, the ANSYS AUTODYN explosion mechanics analysis software was used for the numerical simulation for the shaped charge jet forming and penetrating the steel target. The effects of the liner thickness, cone angle, and charging length-to-diameter ratio on shaped charge jet performance were analyzed. The optimal combination of these structural parameters was determined by the orthogonal optimization design. The optimized shaped charge structure could penetrate a 105 mm-thick steel target under simulation conditions. The explosion tests determined the average and maximum penetration depths of the main charge of 86.67 and 100 mm, respectively. The minimum and average relative discrepancies between the explosion test and numerical simulation results were 4.76% and 17.46%, respectively. This study provided theoretical and technical support for the optimization design and engineering application of small-caliber shaped charges.

Keywords: small caliber shaped charge, structural parameters, penetration capability, shaped charge jet.

Received November 3, 2022

Accepted April 15, 2024



This article is an Open Access article distributed under the terms and conditions of the Creative Commons Attribution 4.0 (CC BY 4.0) License (<http://creativecommons.org/licenses/by/4.0/>).